LAWRENCE
LIVERMORE
NATIONAL
LABORATORY

LLNL-JRNL-691558

Stability of numerous novel potassium chlorides at high pressure

W. Zhang, A. Oganov, S. Lobanov, E. Stavrou, A. F. Goncharov

May 10, 2016

Scientific Reports

Disclaimer

Stability of numerous novel potassium chlorides at high pressure

Weiwei Zhang[1, 2, †], Artem R. Oganov[2-5, †]
Sergey Lobanov[6, 7,8], Elissaios Stavrou[6,9], Alexander F. Goncharov[6, 8]

K-Cl is a simple system displaying all four main types of bonding, as it contains (i) metallic potassium, (ii) elemental chlorine made of covalently bonded Cl_2 molecules held together by van der Waals forces, and (iii) an archetypal ionic compound KCl. The charge balance rule, assigning classical charges of "+1" to K and "-1" to Cl, predicts that no compounds other than KCl are possible. However, our quantum-mechanical variable-composition evolutionary simulations predict an extremely complex phase diagram, with new thermodynamically stable compounds K_3Cl, K_2Cl, K_3Cl_2, K_4Cl_3, K_5Cl_4, K_3Cl_5, KCl_3, KCl_7.Of particular interest are 2D-metallic homologs $K_{n+1}Cl_n$, the presence of positively charged Cl atoms in KCl_7, and the predicted stability of KCl_3 already at the atmospheric pressure and zero Kelvin. We have synthesized cubic $Pm\bar{3}n$ -KCl_3 at 40-70 GPa and trigonal $P\bar{3}c1$ - KCl_3 at 20-40 GPa in a laser-heated DAC at temperature exceeding 2000 K from KCl and Cl_2.These phases have been identified using in situ combined synchrotron X-ray diffraction and Raman spectroscopy measurements compared to the theory predictions. Upon unloading to 10GPa, $P\bar{3}c1$ - KCl_3 transforms to a yet unknown structure before final decomposition to KCl and Cl_2 at near-ambient conditions.

Recent *ab initio* calculations predicted the formation of unexpected novel high-pressure compounds in several simple systems, such as Li-H[1,] Mg-O[2], and Na-Cl[3]. Three of these systems were subsequently explored experimentally: while so far the predictions

[1]Department of Applied Physics, China Agricultural University, Beijing, 100080, P.R.China. [2]Department of Geosciences, Center for Materials by Design, and Institute for Advanced Computational Science, State University of New York, Stony Brook, NY 11794-2100.

[3]Skolkovo Institute of Science and Technology, Skolkovo Innovation Center, 5 Nobel St., Moscow 143026, Ruassia.[4]Moscow Institute of Physics and Technology, 9 Institutskiy Lane, Dolgoprudny city, Moscow Region 141700, Russia. [5]Northwestern Polytechnical University, Xi'an 710072, China. [6]Geophysical Laboratory, CIW, 5251 Broad Branch Road, Washington, D.C. 20015, USA. [7]V.S. Sobolev Institute of Geology and Mineralogy, SB RAS, 3 Pr. Ac. Koptyga, Novosibirsk 630090, Russia. [8]Center for Energy Matter in Extreme Environments and Key Laboratory of Materials Physics, Institute of Solid State Physics, Chinese Academy of Sciences, 350 Shushanghu Road, Hefei, Anhui 230031, China. [9]Lawrence Livermore National Laboratory, Physical and Life Sciences Directorate, P.O. Box 808 L-350, Livermore, California 94550, USA

†These authors contributed equally to this work.

have not been verified for Li-H[4], for Na-Cl and MgO the predicted compounds ($NaCl_3$, Na_3Cl, and MgO_2) have been confirmed experimentally[3, 5], while more stable NaH_x compounds than originally predicted by Zurek et al[6] have been synthesized and theoretically verified[7], revealing dramatic changes of chemistry under pressure. Here we study K-Cl, a system closely related to Na-Cl and find even richer chemistry and new phenomena.

The only known potassium chloride, KCl, has been extensively studied under pressure, both experimentally[8-10] and using *ab initio* simulations[11-13]. Two crystal structures are known for KCl: the rocksalt-type (B1) structure and cesium chloride-type (B2) structure, the latter becoming stable at ~2 GPa. The same transition occurs in NaCl, but at a much higher pressure of 30 GPa[14-15], reflecting the general tendency for phase transitions to occur at lower pressures for compounds of heavier elements. Yet, as we find, the K-Cl system has a much richer chemistry than Na-Cl. Here we study the K-Cl system using variable-composition evolutionary structure prediction methodology USPEX[16-19], searching for the stable compounds and their corresponding crystal structures (see Methods). In each of these calculations, all possible chemical compositions were allowed with up to 16 atoms in the unit cell, and calculations were performed at pressures of 1 atm, 10 GPa, 35 GPa, 50 GPa, 100 GPa, 150 GPa, 200 GPa, 250 GPa and 300 GPa. The existence of novel Cl-rich compounds has been experimentally verified by performing synthesis of two KCl_3 compounds in a laser-heated diamond anvil cell (DAC).

Results and Discussion

The pressure-composition phase diagram predicted in our calculations (Fig. 1, see also Supporting Online Materials) contains a surprisingly large number of new stable compounds. By thermodynamically stable we mean a compound which is more stable than any isochemical mixture of the elements or other compounds – this definition leads to the convex hull construction shown in Fig. 1b, The dynamical stability of the newly predicted phases was checked and confirmed by phonon calculations (see Supporting Online Material).

To verify these predictions, we performed high-pressure experiments on the K-Cl system in a laser-heated DAC up to 70 GPa in the presence of excess chlorine. We specifically targeted the synthesis of KCl_3, which was predicted to become stable at the lowest pressures. The reaction products were examined by visual observations, Raman confocal spectroscopy, and synchrotron x-ray diffraction (XRD) probes at room temperature (see Supporting Online Material). Combining experimental and theoretical approach was critical to refine the K-Cl phase diagram as several KCl_3 phases showed competing enthalpies in the 0-30 GPa pressure range.

The phase diagram shows that KCl remains stable in the whole pressure range investigated here, but many new compounds become stable at elevated pressures. Perhaps most unexpected is the prediction that KCl_3 is stable already at 1 atm at 0 K. The structure belongs to *P*31*m* space group with 3 formula units (f.u.) in the unit cell (Fig. 2a), and contains exotic trichloride-ions Cl_3^-.The *P*31*m* phase is a semiconductor, with a DFT band gap of 2.60eV. The first phase transition is to the *Pnma* structure at 1.3

GPa. *Pnma* structure has 4 f.u. in the unit cell and also contains trichloride-ions (Fig.2b). Bader analysis gives the charge configuration $K^{+0.83}[Cl^{-0.28}Cl^{-0.04}Cl^{-0.51}]^{-0.83}$, nearly the same as for *Pnma*-$NaCl_3$ [Ref. 3]. $[Cl_3]^-$ion is an isoelectronic analogue of the well-known triiodide-ion $[I_3]^-$ (for example, compound KI_3 is well known), Br_3^- and $ClICl^-$ ions, and can be also related to the known $[Li_3]^-$[Ref. 20] and hypothetical $[H_3]^-$[Ref. 4]ions.

At 9.3 GPa $P\bar{3}c1$ structure of KCl_3 with 6 f.u. (Fig. 2c) in the unit cell becomes energetically favored. The band gap of $P\bar{3}c1$ KCl_3 is 1.78 eV at 20 GPa by DFT calculation. Interestingly, at P > 160 GPa $P\bar{3}c1$ KCl_3 turns metallic due to the band gap closure. Metallic $Pm\bar{3}n$ -KCl_3, isostructural with stable $Pm\bar{3}n$ -$NaCl_3$, is also energetically competitive under pressure. At pressures above 140 GPa and 225 GPa, new chlorine-rich compounds become stable as well K_3Cl_5 and KCl_7, respectively.

We synthesized KCl_3 at elevated pressures and temperatures at conditions of excess of Cl_2. To overcome the kinetic barriers, the reagents were laser-heated above 2000 K. The temperature was determined radiometrically. This heating procedure also promotes better mixing of reagents as chlorine melts and becomes highly diffusive.

Pressures in excess of 20 GPa were necessary to initiate a chemical reaction between KCl and Cl_2. A set of new Bragg peaks was observed after laser heating at 20-40GPa with intensities and angular positions in agreement with $P\bar{3}c1$ KCl_3 (Fig. 3).Rietveld refinement, however, was not possible because of the apparent texturing of new reflections (Fig. S4).A rich Raman spectrum, with at least 15 peaks (Fig. 3),was observed for the synthesized compound, which is consistent with the group theory allowing 16 Raman active modes ($\Gamma = 5A_{1g} + 11\ E_g$) for $P\bar{3}c1$ KCl_3. Likewise, Raman shift of the experimentally observed bands agrees with that computed for $P\bar{3}c1$ KCl_3

at corresponding pressures(Fig. S5).Therefore, experiments confirm that $P\bar{3}c1$ KCl_3 is the most stable phase in the 20-40 GPa pressure range.

XRD of quenched samples prepared at P >35-40GPa shows a mixture of two space-separated phases of KCl_3: $P\bar{3}c1$ and $Pm\bar{3}n$. Larger yields of the new phase were achieved at P > 50-60 GPa in qualitative agreement with theoretical predictions showing that the energy difference between $P\bar{3}c1$ and $Pm\bar{3}n$ KCl_3 decreases with increasing pressure. We could only use the LeBail refinement of $Pm\bar{3}n$ KCl_3 because of the spotty character of XRD images (Fig. S6).

The agreement between the experimentally measured and computed equations of state of KCl_3 (Fig. 3d) further validates theoretical predictions.

It is remarkable that in a number of experiments KCl reacted completely, forming KCl_3, with the only remaining material in the probed area being *Cmca*-chlorine, which was easily characterized based on experimental[21], and our theoretically calculated lattice parameters.

On decompression to below 10 GPa, Raman bands of $P\bar{3}c1$ KCl_3 disappeared completely while new strong and pressure-dependent bands appeared near 450 cm^{-1} (Fig. S7). We tentatively assigned these bands to the stretching vibrations of the linear Cl_3^-ions[22]. Changes in XRD also suggest a phase transition, although the quality of the diffraction pattern was not sufficient to index new peaks and pinpoint the structure. At room temperature, this new phase becomes unstable below 4 GPa: Raman spectroscopy, X-ray diffraction and visual observations showed only the presence of KCl and Cl_2 in the decompressed sample cavity.

In the K-Cl system, in contrast with Na-Cl, there is yet another chlorine-rich phase, $P\bar{4}$ *m*2- K_3Cl_5, which has a pseudocubic cell with 1 formula unit. The K atom in the center of the unit cell is surrounded by 4 K atoms and 10 Cl atoms, together forming a

bicapped hexagonal antiprism (Fig. 2f). The electronic structure (Fig. 4) shows that it is a poor metal with a deep pseudogap of width ~4.6 eV at 240 GPa. In Fig. 4 we compare the total and atom-projected electronic densities of states of $P\bar{4}m2$-K_3Cl_5, $Pm\bar{3}n$ -KCl_3 and $Pm3$-KCl_7. All these phases are poor metals with pronounced pseudogaps at the Fermi level, implying electronic stabilization. The main contribution at the Fermi level comes from chlorine atoms, and one can observe that different chlorine sites play very different roles – for example, in $P\bar{4}m2$-K_3Cl_5 only p-orbitals of Cl (4j) contribute at the Fermi level, and are thus responsible for its metallicity. Due to excess of chlorine atoms, which act as electron acceptors, $Pm\bar{3}n$ -KCl_3 has DOS similar to p-type semiconductors. The central, positively charged Cl atom, donating electrons to the system in $Pm3$-KCl_7, makes the DOS at the Fermi level in KCl_7 much higher than that in $P\bar{4}m2$-K_3Cl_5 and $Pm\bar{3}n$ -KCl_3. Distributions of valence electron localization function (ELF, e.g., Fig. 4b) indeed show that crystallographically inequivalent Cl atoms have very different ELF distributions – from spherical (around atoms with the most negative Bader charge, indicating a closed-shell configuration, and also around the positively charged Cl atom in KCl_7) to toroidal (around atoms with small negative charges).

Comparing Bader charges of K-Cl phases (Table 1) with those of Na-Cl phases, we see higher charges on Na atoms in $Pnma$-$NaCl_3$, $Pm\bar{3}n$ -$NaCl_3$ and $Pm3$-$NaCl_7$ (about +0.8) than in their K-counterparts (about +0.65). This is counterintuitive, but consistent with our finding[23] that under pressure K has higher electronegativity and lower reactivity than Na, due to the well-known s→d electronic transition in K atoms under

pressure. Related to this is the observation that the depth of the convex hull (i.e. the enthalpy of formation of KCl or NaCl) in the K-Cl system (Fig. 1) changes from -2.9 eV/atom at 40 GPa to -1.5 eV/atom at 300 GPa, whereas for the Na-Cl system[3] it changes from -2.5 eV/atom at 40 GPa to -2.9 eV/atom at 300 GPa.

In the studied pressure range, besides the known B1 and B2 phases, we find a new phase of KCl: $I4_1/amd$–KCl, stable above 201 GPa, shown in Fig.5a. This structure is a derivative of the fcc structure. Fig.5b shows K_3Cl, the other fcc-derived superstructure compound stable in the K-Cl system (above 149 GPa) – square planar layers with stoichiometry KCl alternate with similar layers of stoichiometry K_2 along the *c*-axis, leading to the total stoichiometry K_3Cl. These two compounds can be described as fcc-based homologs.

There is another interesting and surprisingly rich class of phases, $K_{n+1}Cl_n$ homologs (*n*=2, 3, 4 were found in our calculations, but we cannot exclude the possibility of even larger–*n* homologs) based on the B2 structure and shown in Fig. 5c-g. These have (2*n*+1) layers along the *c*-axis, with extra K-layer serving as an antiphase boundary between B2-structured domains. All these phases have the same space group $I4/mmm$, and similar interatomic distances, all of them are poor metals, due to the excess of electron-donating K atoms, analogous to n-type semiconductors (Fig. S8), and display a two-dimensional metallic character. It is surprising that phases with different *n* have quite different stability fields: e.g., K_2Cl is stable at pressures above 56 GPa, whereas K_5Cl_4 is stable above 100 GPa. Interestingly, mobile electrons are observed only at the antiphase boundaries, whereas regions between them are insulating (Fig. 5g). These

antiphase boundaries may be created as metastable growth defects also at lower pressures, with the promise of new electronic materials.

In summary, for a seemingly simple K-Cl system our calculations predict an extremely unusual behavior. Already at ambient pressure we predict stability of a new insulating compound KCl_3, which has not been observed before. As pressure increases, a surprisingly large number of thermodynamically stable phases become stable: (1) Cl-rich metallic phases (KCl_7, K_3Cl_5, and a metallic form of KCl_3) with high coordination numbers (12-14), (2) fcc-superstructures (insulating $I4_1/amd$ KCl and metallic K_3Cl), (3) layered B2-superstructures with compositions $K_{n+1}Cl_n$(n=3,4,5) and two-dimensional electronic conductivity. Our experiments confirmed stability of two new forms of KCl_3, $Pm\bar{3}n$ and $P\bar{3}c1$- KCl_3, which were synthesized in the laser diamond anvils cell from KCl and Cl_2. KCl_3 decomposes into KCl and Cl_2 at room temperature at pressures below 4GPa and probably is stable at zero pressure and low temperatures, as suggested by theory. What was considered as an ultimately simple chemical system, upon careful theoretical and experimental study turned out to be a very rich system with novel physics and chemistry? Revisiting other simple systems may result in the formulation of new chemical principles that could be used for the discovery of novel materials and phenomena.

Author contribution:

A.R.O. designed the research. W.W.Z. and A.R.O. performed the calculations, interpreted data and wrote the paper. A. F. G, E. S., and S. L. designed and performed the experiments, reduced and interpreted the data and contributed to writing the manuscript.

Acknowledgments

We thank Xiao Dong for discussions, NSCF (Grant No. 11474355), Chinese Universities Scientific Fund (Grant No. 2015LX002), DaBeiNong Young Scholars Research Plan, DARPA (Grant No. W31P4Q1210008) and the Government (No. 14.A12.31.0003) of Russian Federation, and Foreign Talents Introduction and Academic Exchange Program (No. B08040). A. F. G. acknowledges support from the Army Research Office, DARPA, and NSF EAR. X-ray diffraction experiments were performed at GeoSoilEnviroCARS (Sector 13), Advanced Photon Source (APS), Argonne National Laboratory and Petra III, DESY, Hamburg, Germany. GeoSoilEnviroCARS is supported by the National Science Foundation - Earth Sciences **(**EAR-1128799) and Department of Energy - Geosciences (DE-FG02-94ER14466).The research leading to these results has received funding from the European Community's Seventh Framework Programme (FP7/2007-2013) under grant agreement n° 312284. Use of the Advanced Photon Source was supported by the U. S. Department of Energy, Office of Science, Office of Basic Energy Sciences, under Contract No. DE-AC02-06CH11357.PETRA III at DESY is a member of the Helmholtz Association (HGF). S. L. was partly supported by the Ministry of Education and Science of Russian Federation (No 14. B25.31.0032). We thank V. Prakapenka and Z. Konopkova for the excellent technical support. Work of E.S. was performed under the auspices of the U. S. Department of Energy by Lawrence Livermore National Security, LLC under Contract DE-AC52-07NA27344.

References:

1. Zurek, E., Hoffmann, R., Ashcroft, N.W., Oganov, A.R., Lyakhov, A.O. A little bit of lithium does a lot for hydrogen. *Proc.Natl.Acad.Sci.***106**:17640-17643 (2009).

2. Zhu, Q., Oganov, A.R., Lyakhov, A.O. Novel stable compounds in the Mg-O system underhighpressure. *Phys. Chem. Chem. Phys.* **15**:7796-7700 (2013).

3. Zhang, W.W., *et al.* Unexpected stoichiometries of stable sodium chlorides. *Science* **342**: 1502-1505 (2013).

4. Howie, R.T., Narygina, O., Guillaume, C.L. High-pressure synthesis of lithium hydride. *Phys Rev B* **86**:064108 (2012)

5. Lobanov S.S., *et al.* Stable magnesium peroxide at high pressure. *Scientific Reports* **5**: 13582 (2015).

6. Hooper, J.&Zurek, E. Lithium Subhydrides under pressure and their superatom-like building blocks. *Chem. Phys. Chem*. **77**:969-972 (2012).

7. Struzhkin et al, Nature Comm., under review.

8. Campbell, A.J., Heinz, D.L. Compression of KCl in the B2 structure to 56 GPa. *J. Phys. Chem. Solids* **52**:495–499(1991).

9. Hofmeister, A.M. IR Spectroscopy of alkali halides at very high Pressures: calculation of equation of state and the response of bulk moduli to the B1 → B2 phase transition. *Phys. Rev. B* **56**:5835–5855 (1997).

10. Al'tshuler, L.V., Pavlovskii, M.N., Kuleshova, L.V., Simakov, G.V. Investigation of alkali-metal halides at high pressures and temperatures produced by shock compression. *SovPhys-Solid State* **5**:203 (1963).

11. Durandurdu, M. Ab initio molecular dynamics study of pressure-induced phase transformation in KCl. *Comp. Mater. Sci.***48**: 672–676 (2010).

12. Recio, J.M., Pendás, A. M., Francisco, E., Flórez, M., Luaña, V. Low pressure and high pressure equations of state for the alkali chlorides. *Phys. Rev. B* **48**:5891–5901(1993).

13. Sims, C.E., Barrera, G.D. Thermodynamics and mechanism of the B1-B2 phase transition in group-I halides and group-II oxides. *Phys. Rev. B* **57**:11164(1998).

14. Bassett, W. A., Takahash, T., Mao, H. K., Weaver, J. S. Pressure-induced phase transformation in NaCl. *J. Appl. Phys.* **39**:319 (1968).

15. Froyen, S., Cohen, M. L. Structural properties of NaCl.*Phys. Rev. B* **29**: 3770 (1984).

16. Oganov, A.R., Glass, C.W. Crystal structure prediction using *ab initio* evolutionary techniques: Principles and applications. *J. Chem. Phys.***124**: 244704 (2006).

17. Lyakhov, A.O., Oganov, A.R., Stokes, H.T., Zhu, Q. New developments in evolutionary structure prediction algorithm USPEX. *Comp. Phys. Comm.***184**:1172-1182 (2013).

18.Oganov,A.R., Lyakhov,A.O., ValleM. How evolutionary crystal structure prediction works - and why. *Acc. Chem. Res.***44**:227-237 (2011).

19.Oganov, A.R., Ma, Y.M., Lyakhov, A.O., Valle, M., Gatti, C. Evolutionary crystal structure prediction as a method for the discovery of minerals and materials. *Rev. Mineral Geochem.***71**:271-298 (2010).

20. Gole, J. L., Childs, R. H., Dixon, D. A., Eades, R. A. The electronic structure of the lithium trimer anion and cation. *J. Chem. Phys.***72**: 6368 –6375 (1980).

21.Fujihisa H., FujiiY., Takemura K., Shimomura O. Structural aspects of dense solid halogens under high pressure studied by X-ray diffraction molecular dissociation and metallization. *J. Phys. Chem. Solids* **56:**1439-1444 (1995)**.**

22. Ault B.S., Andrews L. Infrared and Raman spectra of the $M^{+}Cl^{3-}$ ion pairs and their chlorine–bromine counterparts isolated in argon matrices. *J. Chem. Phys.***64**: 4853-4859 (1976).

23. Dong X., *et al.* How do chemical properties of the atoms change under pressure? under review.

24. Perdew, J.P., Burke, K., Ernzerhof, M. Generalized gradient approximation made simple. *Phys. Rev. Lett.***78**:3865-3868 (1996).

25. Kresse, G., Furthmuller, J. Efficiency of *ab initio* total energy calculations for metals and semiconductors using a plane-wave basis set. *Comp. Mater. Sci.***6**:15-50 (1996).

26. Blochl, P.E.Projector augmented-wave method. *Phys. Rev. B* **50**: 17953-17979 (1994).

27. Valle, M. STM3: a chemistry visualization platform. *Z. Kristallogr.***220**:585-588 (2005).

Figure 1. Stability of new potassium chlorides: (a) Pressure-composition phase diagram of the K-Cl system. (b) Convex hull diagrams for the K-Cl system at selected pressures. Solid circles represent stable compounds; open circles - metastable ones.

Figure 2.Crystal structures of (a) *P*31*m*-KCl_3 at 1atm, (b) *Pnma*-KCl_3 at 5GPa (c) $P\bar{3}c1$- KCl_3 at 20GPa, (d) $Pm\bar{3}n$-KCl_3 at 240 GPa, (e) *Pm*3-KCl_7 at 240GPa, (f) $P\bar{4}m2$-K_3Cl_5 at 240 GPa.

Figure 3. Experimental evidence for KCl_3: (a) XRD pattern of $P\bar{3}c1$- KCl_3 and Cl_2 at 21 GPa, (b) Raman spectrum of reaction products after laser-heating at 22 GPa. Purple bars show computed spectral positions of $P\bar{3}c1$- KCl_3 at 20 GPa, (c) X-ray diffraction pattern of $Pm\bar{3}n$- KCl_3, KCl, and Cl_2 at 57 GPa. (d) Experimental and theoretical pressure-volume equations of state of $P\bar{3}c1$ and $Pm\bar{3}n$-KCl_3. In (a) and (c) black lines show the intensity difference (I_{obs}-I_{calc}), Le Bail refinement residuals are R_{wp} = 0.139 and R_{exp} = 0.096 in (a) and R_{wp} = 0.233 and R_{exp} = 0.151 in (c). X-ray wavelengths are 0.3100 Å in (a) and 0.3344 Å in (c).

Figure 4. Electronic structure: (a) band structure and electronic density of states of $P\bar{4}m2$- K_3Cl_5 at 240 GPa, (b) electron localization function of $P\bar{4}m2$-K_3Cl_5 at 240 GPa with isosurface ELF=0.77. (c) total and atom-projected densities of states of $P\bar{4}m2$-K_3Cl_5, (d) total and atom-projected densities of states of $Pm\bar{3}n$-KCl_3, (e) total and atom-projected densities of states of *Pm*3-KCl_7 at 240 GPa.

Figure5. Crystal structures of (a) high-pressure $I4_1/amd$-KCl, (b) fcc-derived *I*4/*mmm*-K_3Cl, and bcc-derived $K_{n+1}Cl_n$ homologs: (c) *I*4/*mmm*-K_2Cl,(d)

*I*4/*mmm*-K_3Cl_2, (e)*I*4/*mmm*-K_4Cl_3, (f) *I*4/*mmm*-K_5Cl_4 (g) Spatial distribution of electrons (shown by isosurfaces and density contours) at the Fermi level in *I*4/*mmm*-K_5Cl_4, showing clear 2D-metallic character.

Table 1. Structures of B1-KCl and *P*31*m*-KCl_3 at 1 atm, *Pnma*-KCl_3 at 5GPa, $P\bar{3}c1$-KCl_3 and B2-KCl at 20 GPa, A15-type ($Pm\bar{3}n$) KCl_3, *Pm*3-KCl_7 , $P\bar{4}m2$-K_3Cl_5, *I*4/*mmm*-K_3Cl and $I4_1/amd$-KCl at 240 GPa, and the corresponding atomic Bader charges (Q) and volumes (V).

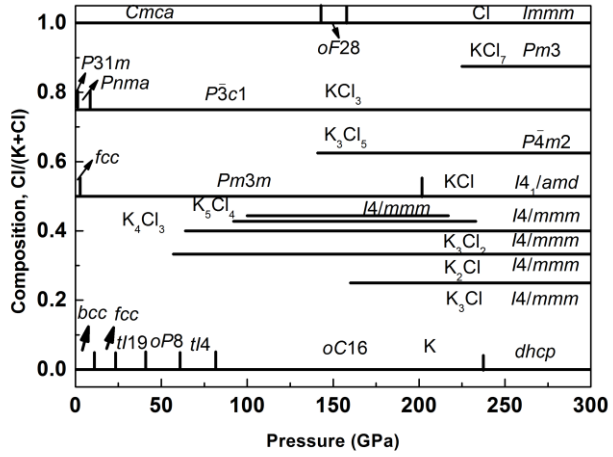

(a)

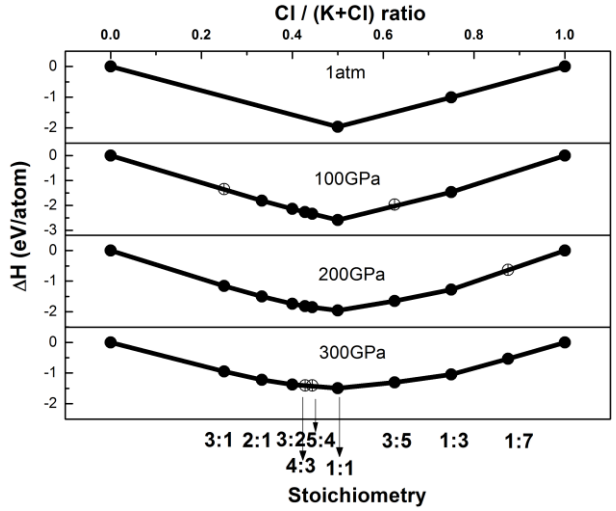

(b)

Figure 1. Stability of new potassium chlorides: (a) Pressure-composition phase diagram of the K-Cl system. (b) Convex hull diagrams for the K-Cl system at selected pressures. Solid circles represent stable compounds; open circles - metastable ones.

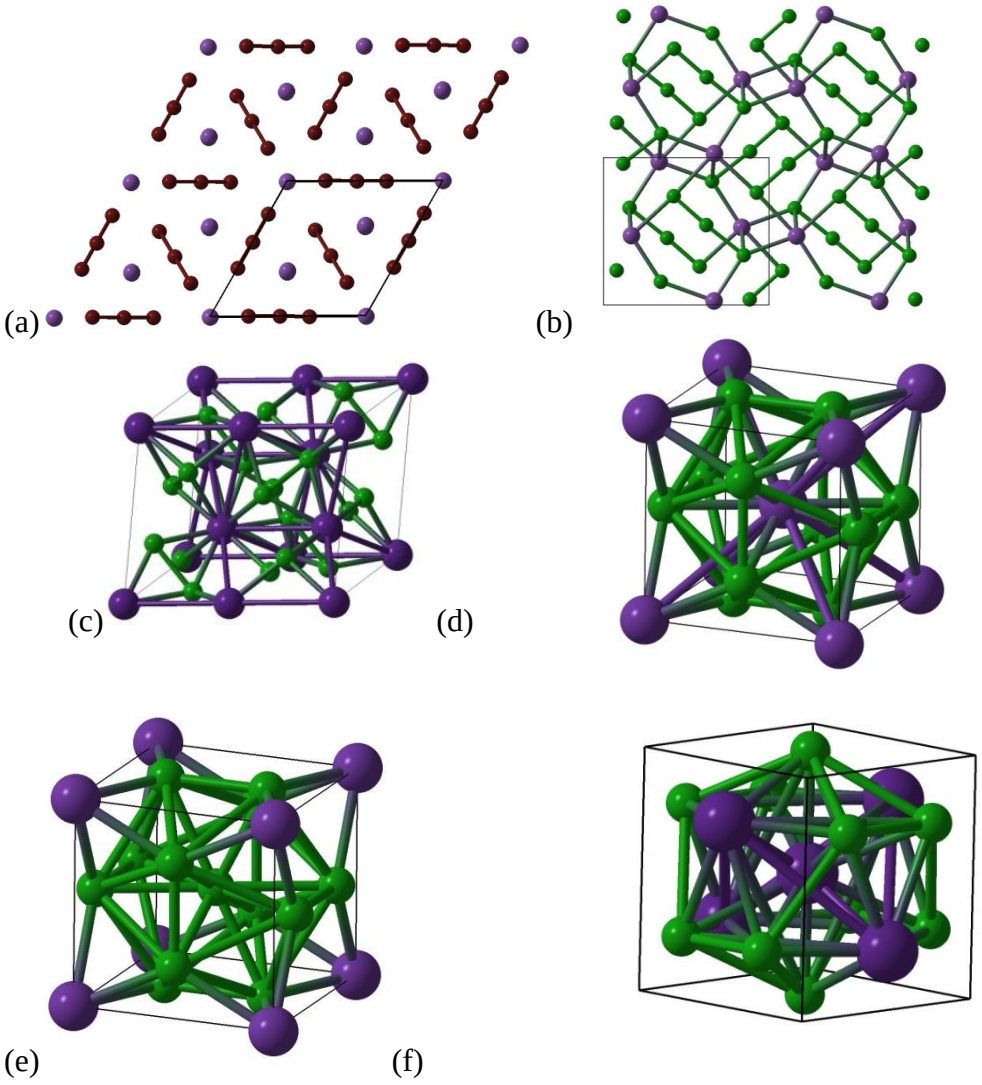

Figure 2. Crystal structures of (a) *P*31*m* at 0GPa, (b) *Pnma*-KCl_3 at 5 GPa, (c) $P\bar{3}c1$ - KCl_3 at 20 GPa, (d) $Pm\bar{3}n$-KCl_3 at 240 GPa (e) *Pm*3-KCl_7 at 240 GPa, (f) $P\bar{4}m2$ -K_3Cl_5 at 240 GPa.

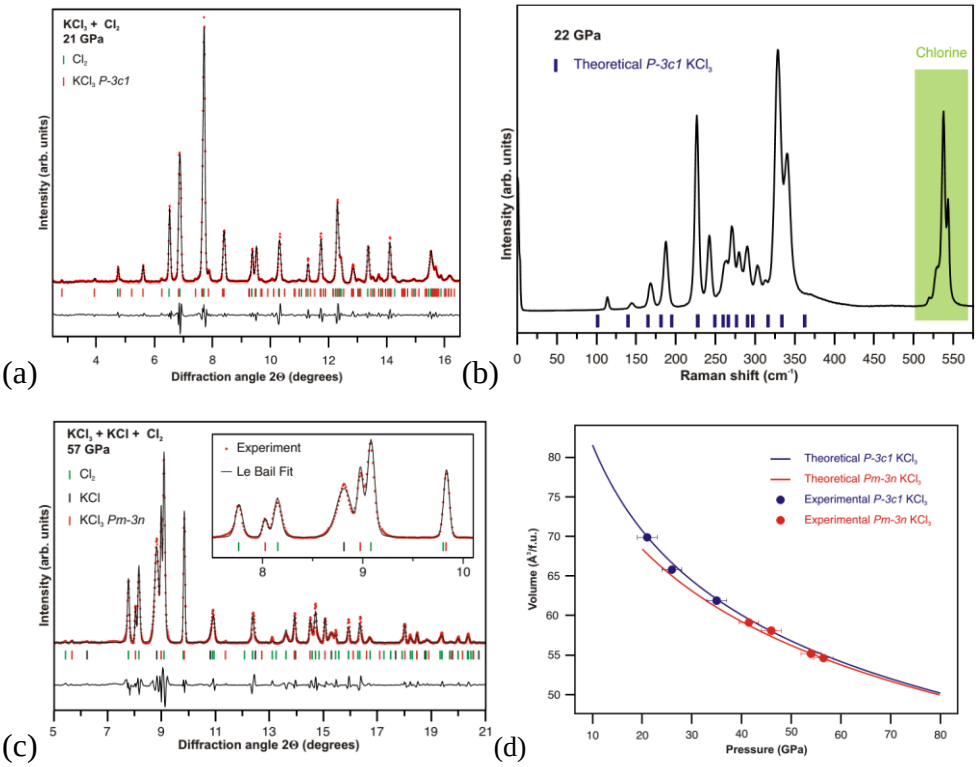

Figure 3. Experimental evidence for KCl_3: (a) XRD pattern of $P\bar{3}c1$- KCl_3 and Cl_2 at 21 GPa, (b) Raman spectrum of reaction products after laser-heating at 22 GPa. Purple bars show computed spectral positions of $P\bar{3}c1$- KCl_3 at 20 GPa, (c) X-ray diffraction pattern of $Pm\bar{3}n$- KCl_3, KCl, and Cl_2 at 57 GPa. (d) Experimental and theoretical pressure-volume equations of state of $P\bar{3}c1$ and $Pm\bar{3}n$-KCl_3. In (a) and (c) black lines show the intensity difference (I_{obs}-I_{calc}), Le Bail refinement residuals are R_{wp} = 0.139 and R_{exp} = 0.096 in (a) and R_{wp} = 0.233 and R_{exp} = 0.151 in (c). X-ray wavelengths are 0.3100 Å in (a) and 0.3344 Å in (c).

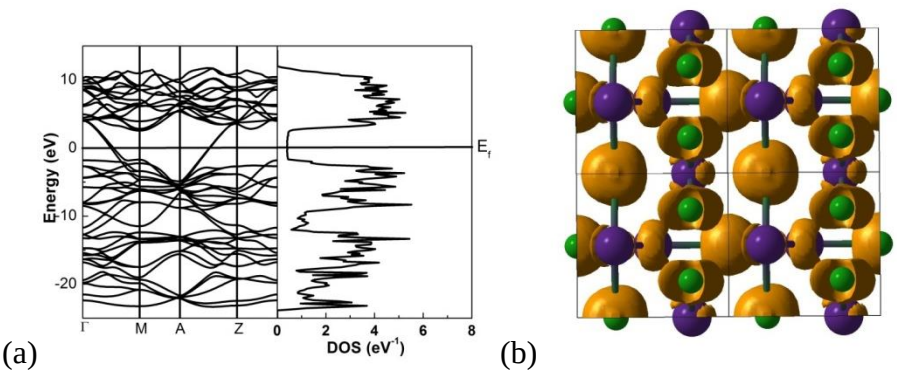

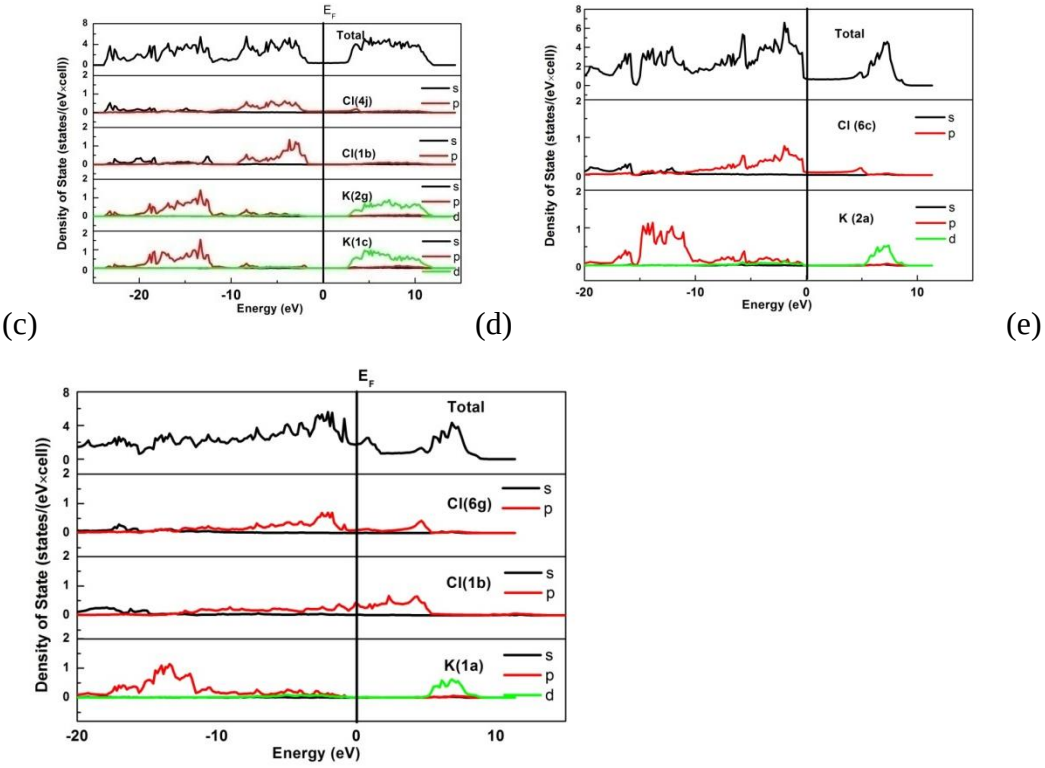

Figure 4. Electronic structure: (a) band structure and electronic density of states of $P\bar{4}m2$-K_3Cl_5 at 240 GPa, (b) electron localization function of $P\bar{4}m2$-K_3Cl_5 at 240 GPa with isosurface ELF=0.77, (c) total and atom-projected densities of states of $P\bar{4}m2$-K_3Cl_5, (d) total and atom-projected densities of states of $Pm\bar{3}n$-KCl_3, (e) total and atom-projected densities of states of $Pm3$-KCl_7 at 240 GPa.

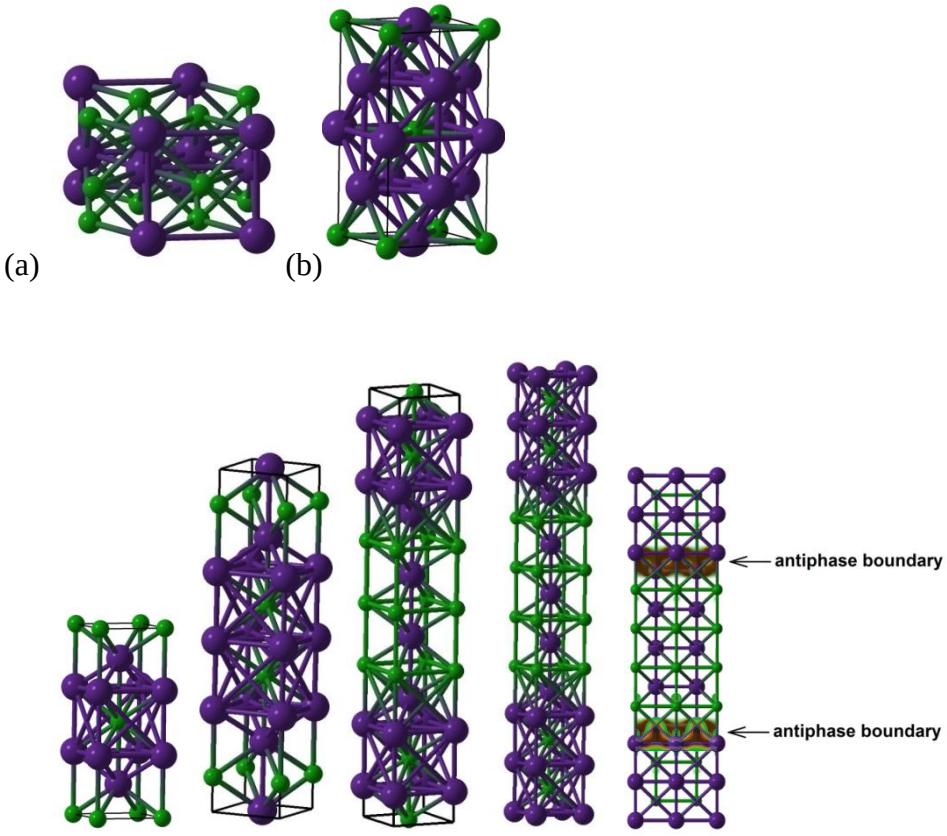

(a) (b) (c) (d) (e) (f) (g)

Figure 5. Crystal structures of (a) high-pressure $I4_1/amd$-KCl,(b) fcc-derived $I4/mmm$-K_3Cl, and bcc-derived $K_{n+1}Cl_n$ homologs:(c) $I4/mmm$-K_2Cl,(d) $I4/mmm$-K_3Cl_2, (e) $I4/mmm$-K_4Cl_3, (f) $I4/mmm$-K_5Cl_4 (g) Spatial distribution of electrons (shown by isosurfaces and density contours) at the Fermi level in $I4/mmm$-K_5Cl_4, showing clear 2D-metallic character.

Table 1. Structures of B1-KCl and *P*31*m*-KCl_3 at 1 atm, *Pnma*-KCl_3 at 5GPa, $P\bar{3}c1$-KCl_3 and B2-KCl at 20 GPa, A15-type ($Pm\bar{3}n$) KCl_3, *Pm*3-KCl_7 , $P\bar{4}m2$-K_3Cl_5, *I*4/*mmm*-K_3Cl and $I4_1/amd$-KCl at 240 GPa, and the corresponding atomic Bader charges (Q) and volumes (V).

	Lattice Parameters		X	y	Z	Q, |e|	V, Å^3
B1-KCl	*a* = 3.192 Å	K(4b)	0.500	0.500	0.500	+0.843	22.88
		Cl(4a)	0.000	0.000	0.000	-0.843	42.17
B2-KCl	*a* = 3.350 Å	K(1a)	0.000	0.000	0.000	+0.784	15.23
		Cl(1b)	0.500	0.500	0.500	-0.784	22.38
Pnma-KCl_3	*a* = 8.708 Å *b* = 5.427 Å c = 7.947 Å	K(4c)	0.827	0.750	0.536	+0.835	18.63
		Cl(4c)	0.933	0.250	0.769	-0.279	25.22
		Cl(4c)	0.162	0.750	0.640	-0.514	26.72
		Cl(4c)	0.878	0.750	0.052	-0.042	23.31
*P*31*m*-KCl_3	*a* = 8.587 Å c =6.206 Å	K(2b)	0.333	0.667	0.000	+0.878	23.43
		K(1a)	0.000	0.000	0.504	+0.876	25.13
		Cl(3c)	0.667	0.667	0.251	-0.404	37.40
		Cl(3c)	0.000	0.512	0.528	-0.049	33.20
		Cl(3c)	0.000	0.693	0.805	-0.424	37.52
$P\bar{3}c1$- KCl_3	*a* = 7.347 Å c = 9.059 Å	K(2b)	0.000	0.000	0.000	+0.780	13.71
		K(4d)	0.333	0.667	0.143	+0.794	14.53
		Cl(6f)	0.260	0.260	0.250	-0.073	17.66
		Cl(12g)	0.289	0.403	0.897	-0.358	19.33
$Pm\bar{3}n$ -KCl_3	*a* = 4.169 Å	K(2a)	0.000	0.000	0.000	+0.519	7.91
		Cl(6c)	0.000	0.500	0.250	-0.173	9.43

*Pm*3-KCl_7	*a* = 4.123 Å	K(1a)	0.000	0.000	0.000	+0.493	7.77
		Cl(1b)	0.500	0.500	0.500	+0.063	8.47
		Cl(6g)	0.745	0.500	0.000	-0.089	8.99
$P\bar{4}m2$-K_3Cl_5	*a* = 4.136 Å *c* = 4.361 Å	K(1c)	0.500	0.500	0.500	+0.566	8.47
		K(2g)	0.500	0.000	0.245	+0.542	8.18
		Cl(1b)	0.500	0.500	0.000	-0.512	10.11
		Cl(4j)	0.252	0.000	0.747	-0.285	9.91
$I4_1/amd$ -KCl	*a* = 3.340 Å *c* = 6.873 Å	K(4a)	0.000	0.250	0.875	+0.545	8.595
		Cl(4b)	0.000	0.750	0.625	-0.545	10.579
I4/mmm-K_3Cl	*a* = 3.365 Å *c* = 6.583 Å	K(2b)	0.500	0.500	0.000	+0.288	8.818
		K(4d)	0.500	0.000	0.250	+0.249	8.863
		Cl(2a)	0.000	0.000	0.000	-0.786	10.726
I4/mmm-K_2Cl	*a*= 2.749Å *c* = 7.587Å	K(4e)	0.000	0.000	0.330	+0.344	9.19
		Cl(2a)	0.000	0.000	0.000	-0.688	11.30
I4/mmm-K_3Cl_2	*a* = 2.801 Å *c* = 12.806 Å	K(2b)	0.500	0.500	0.000	+0.489	9.24
		K(4e)	0.500	0.500	0.798	+0.405	9.12
		Cl(4e)	0.000	0.000	0.897	-0.655	11.39
I4/mmm-K_4Cl_3	*a* = 2.791Å *c* = 18.190Å	K(4e)	0.000	0.000	0.784	+0.413	9.13
		K(4e)	0.000	0.000	0.072	+0.449	9.17
		Cl(2b)	0.000	0.000	0.500	-0.673	11.66
		Cl(4e)	0.000	0.000	0.646	-0.621	11.31
I4/mmm-K_5Cl_4	*a* = 2.789 Å *c* = 23.531 Å	K(2a)	0.000	0.000	0.000	+0.569	9.19
		K(4e)	0.500	0.500	0.612	+0.563	9.13
		K(4e)	0.500	0.500	0.276	+0.410	9.12

	Cl(4e)	0.000	0.000	0.669	-0.622	11.32
	Cl(4e)	0.000	0.000	0.557	-0.636	11.58

Supporting Materials for:

Stability of numerous novel potassium chlorides at high pressure

Weiwei Zhang[1, 2 †], Artem R. Oganov[2-5, †]
Sergey Lobanov[6, 7], Elissaios Stavrou[6], Alexander F. Goncharov[6, 8]

*Corresponding author. E-mail: zwwjennifer@gmail.com (W.W.Z.); artem.oganov@sunysb.edu (A.R.O.)

Supplementary Materials
Methods
Figs.S1 to S9, Table S1.

Methods

Structure/composition predictions were done using the USPEX code[16-18] in the variable-composition mode[19]. The first generation of structures was produced randomly and the subsequent generations were obtained by applying heredity, transmutation, softmutation, and lattice mutation operations, with probabilities of 60%, 10%, 20% and 10%, respectively. 60% fittest non-identical structures of each generation were used to produce the next generation. 20% new random symmetric structures were also added in each generation. All structures were relaxed using density functional theory (DFT) calculations at the generalized gradient approximation level of theory, with the Perdew-Burke-Ernzerhof (PBE) [24] exchange-correlation functional, as implemented in the VASP code[25]. We used the all-electron projector augmented wave (PAW) [26] with K [$3s^2 3p^6 4s^1$], Cl [$2s^2 2p^4$] cores (core radii 2.20 a.u. and 1.50 a.u., respectively) and plane-wave basis sets with the 500 eV cutoff, and dense

Monkhorst-Pack meshes with resolution better than $2\pi\times0.05$Å^{-1}. We used the normalized enthalpy of formation as fitness and visualized crystal structures and electron density distributions using the STM4 package[27]. Having identified the most stable compositions and structures, we relaxed them at pressures between 1 atm and 300 GPa using very accurate Brillouin zone sampling (Monkhorst-Pack meshes with resolution of better than $2\pi\times0.03$Å^{-1}).

Experiment: We used symmetrical diamond anvil cells (DAC) to generate static pressures up to 50 GPa. The diamond culet size was 300 μm. Sample chambers were created by laser drilling of 70-80 μm holes in Re gaskets (40 μm thick). Potassium chloride was heated to 130 °C and kept at this temperature for 3-4 hours. Circular platelets matching the dimensions of the gasket hole were placed on each of the diamond anvils. Subsequently, chlorine was loaded in a DAC cooled by liquid nitrogen in a nitrogen-purged glove box. Finally, the DAC was closed and sample brought to high pressure while still at cryogenic temperatures. This loading procedure ensured a 20-30 μm thick chlorine disk confined and isolated from the diamonds by the KCl platelets.

Upon compression, chlorine becomes optically opaque and can be heated directly by a 1075 nm fiber laser. Double-sided laser heating experiments were performed at GeoSoilEnviroCARS (APS, Chicago) and Extreme Conditions Beamline P02.2 at DESY (Germany). Temperature was measured spectroradiometrically. XRD data were collected both at high temperature and from quenched samples. We used an 8 μm x-ray beam to detect phase transformations (chlorine melting, KCl_3 synthesis) at high temperature, while 3-5 μm beam was used to map quenched samples.

Raman radiation was excited using either 488 or 532 nm lines of a solid state laser. The laser spot on the sample was focused to 4 μm. Raman spectra were analyzed with an imaging spectrograph equipped with a charge-coupled device (CCD). The spectral resolution was 4 cm^{-1}.

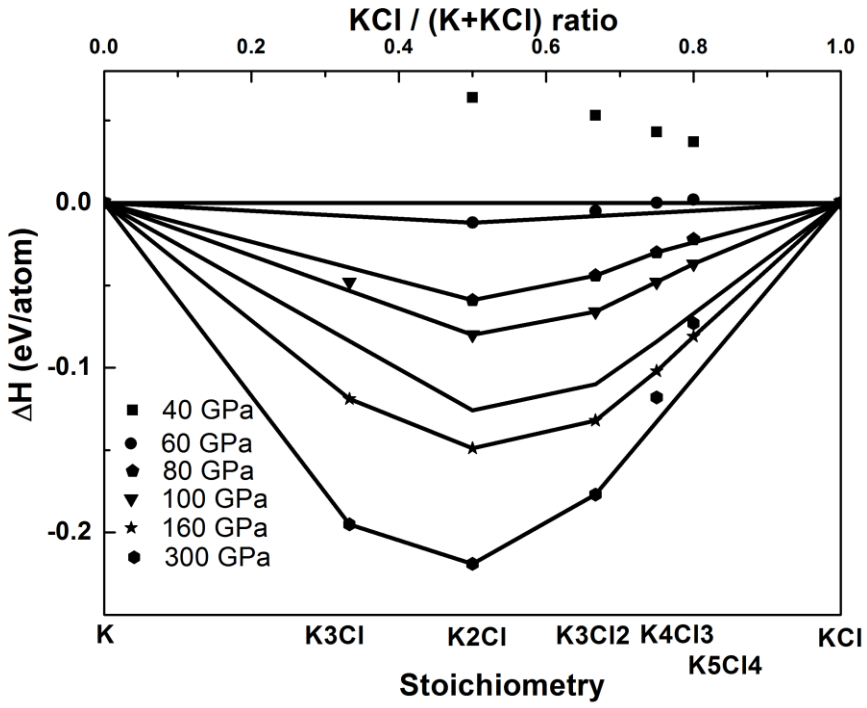

(a)

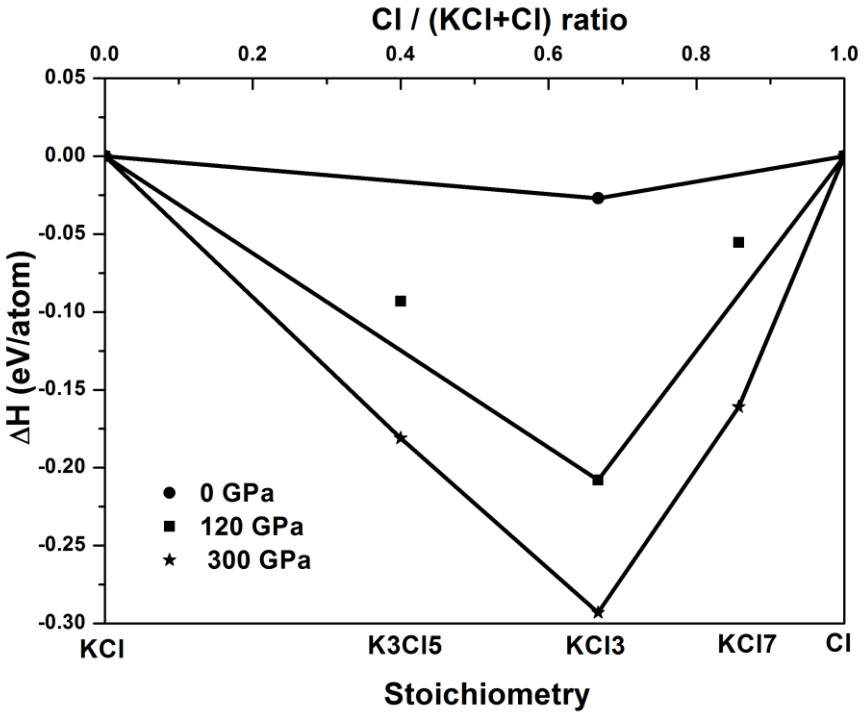

(b)

Figure S1. Convex hull diagrams for (a) K-KCl system and (b) KCl-Cl system.

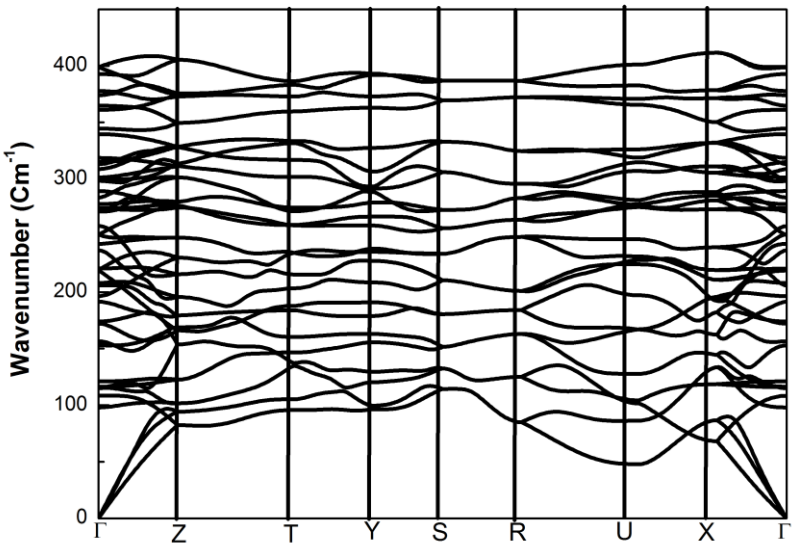

Figure S2. Phonon dispersion curves of *Pnma*- KCl_3 at 30 GPa. Such calculations were done for all predicted structures to ensure their dynamical stability.

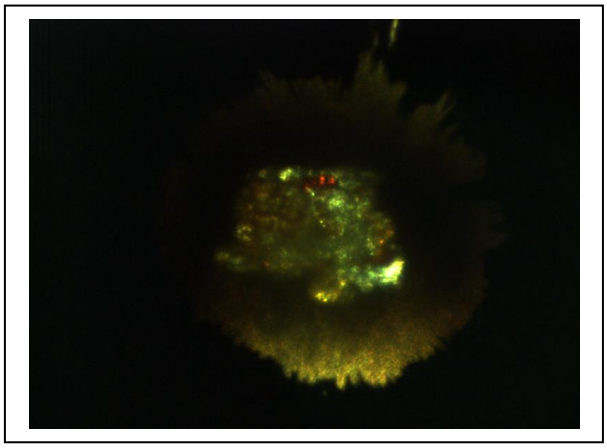

Figure S3. Microphotograph of KCl+Cl_2 sample in the DAC cavity after laser heating at 40 GPa. The formation of new microcrystalline material is seen in the central area, which is surrounded by yellowish Cl_2 unreacted sample.

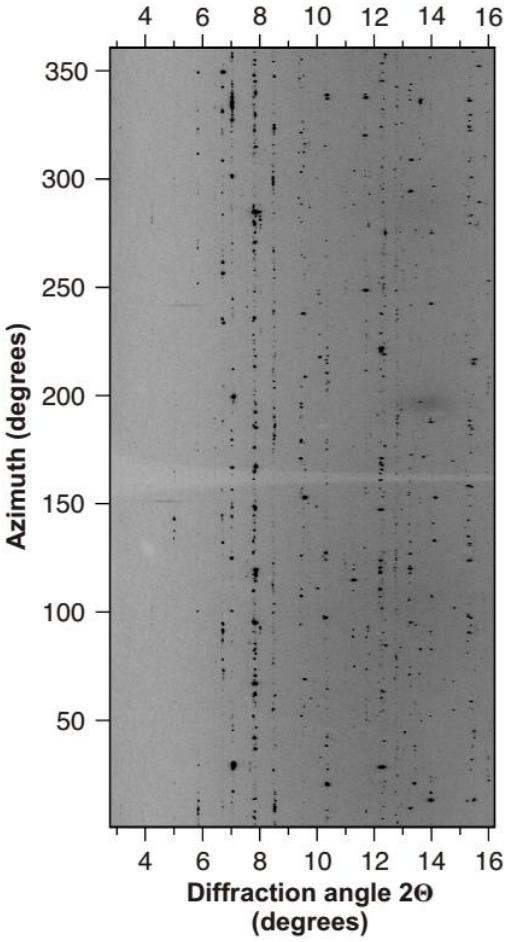

Figure S4. Caked X-ray diffraction image of $P\bar{3}\,c1$ - KCl_3 and Cl_2 at 22 GPa corresponding to Figure 3. The highly textured pattern of KCl_3 precluded Rietveld refinement. The wavelength is 0.3100 Å.

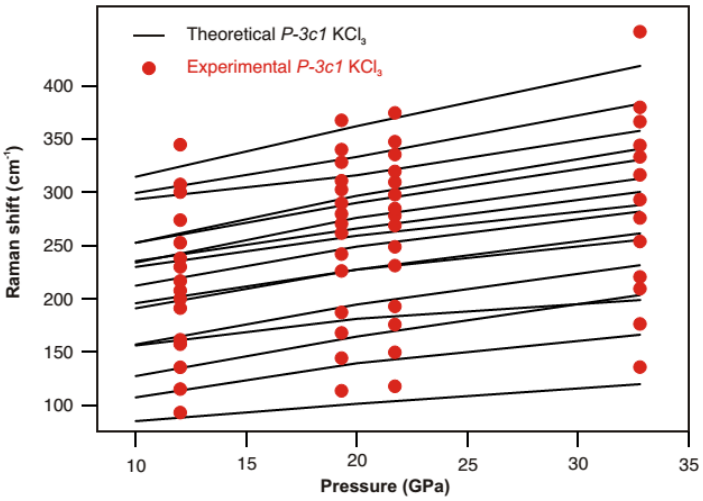

Figure S5. Pressure dependence of the experimentally observed vs theoretically computed $P\bar{3}\,c1$ - KCl_3 Raman bands.

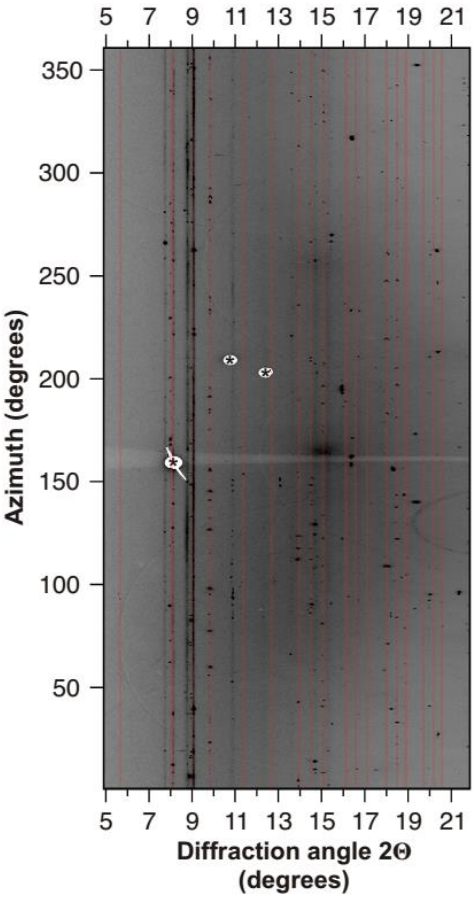

Figure S6. Caked X-ray diffraction image of $Pm\bar{3}n$-KCl_3, KCl, and Cl_2 at 57GPa corresponding to Figure 3. KCl and Cl_2 form quasi-continuous diffraction lines, whereas $Pm\bar{3}n$ KCl_3 shows a highly textured pattern (red lines). White areas marked with an asterisk mask saturated areas of the imaging plate. The wavelength is 0.3344 Å.

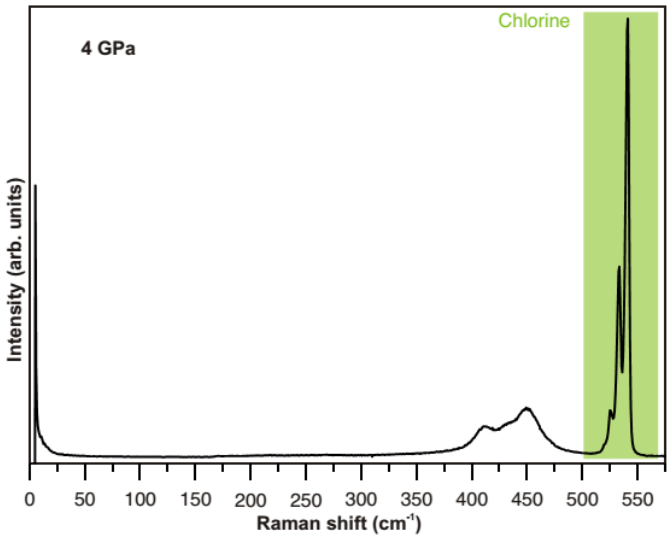

Figure S7. Raman spectrum of a yet unknown K-Cl compound appearing on decompression to P < 10 GPa at 300 K. Chlorine peaks are in the shaded green area.

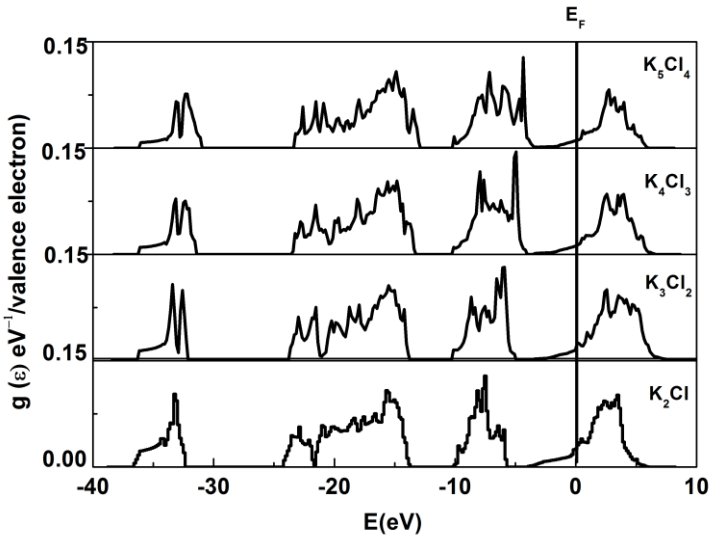

Figure S8. The electronic density of states of layered $K_{n+1}Cl_n$ homologs at 200 GPa.

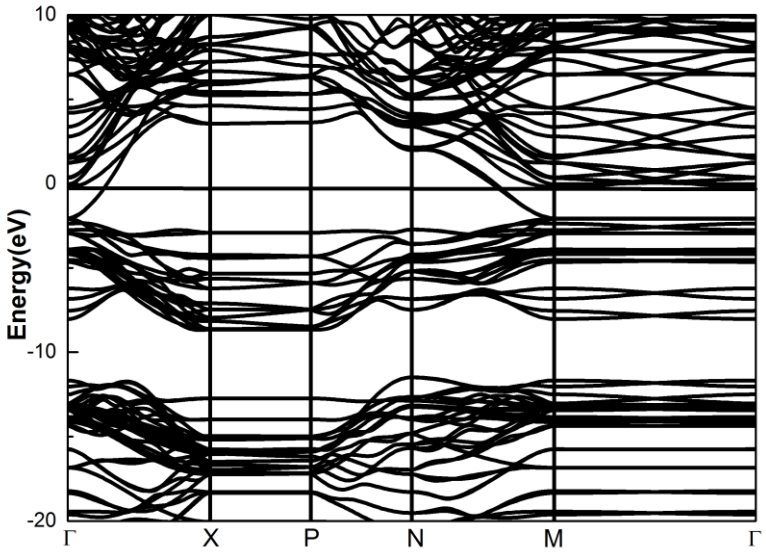

Figure S9. Band structure of *I*4/*mmm*-K_5Cl_4 at 200 GPa.

Table S1. Structure information and corresponding stability pressure regions for new compounds

Class of phases	Composition	Pressure range of stability	Space group	Cell parameters and atomic coordinates	
Insulating KCl	post-B2-KCl	201-300	$I4_1/amd$	a = 3.368 Å c = 6.955 Å (220 GPa)	K1 4a (0.000, 0.250, 0.875) Cl1 4b (0.000, 0.750, 0.625)
Insulating Cl-rich phase	KCl_3	0-1.3	$P31m$	a = 8.587 Å c = 6.206 Å （1atm)	K1 1a (0.000, 0.000, 0.504) K2 2b (0.333, 0.667, 0.000) Cl1 3c (0.667, 0.667, 0.251) Cl2 3c (0.000, 0.512, 0.528) Cl3 3c (0.000, 0.693, 0.805)
	KCl_3	1.3-9.3	$Pnma$	a = 8.708 Å b = 5.426 Å c = 7.946 Å (5 GPa)	K1 4c (x, 0.250, z) x=0.173, z= 0.464 Cl1 4c (x, 0.250, z) x = 0.933, z = 0.769 Cl2 4c (x, 0.250, z) x = 0.622, z = 0.552 Cl3 4c (x, 0.250, z) x = 0.838, z = 0.360
Insulating and metallic Cl-rich phase	KCl_3	9.3-300	$P\bar{3}c1$	a = 7.347 Å c = 9.059 Å (20 GPa)	K1 2b (0.000, 0.000, 0.000) K2 4d (0.333, 0.667, z) z = 0.143 Cl1 6f (x, x, 0.250) x = 0.260 Cl2 12g (x, y, z) x=0.289, y=0.403,z= 0.897
Metallic Cl-rich phases	KCl_3	34-300	$Pm3n$	a = 4.169 Å (240 GPa)	K 2a (0.000, 0.000, 0.000) Cl 6c (0.000, 0.500, 0.250)
	KCl_7	225-300	$Pm3$	a = 4.123 Å (240 GPa)	K 1a (0.000, 0.000, 0.000) Cl1 1b (0.500, 0.500, 0.500) Cl2 6g (x, 0.500, 0.000) x=0.745
	K_3Cl_5	142-300	$P\bar{4}m2$	a = 4.136 Å c = 4.361 Å (240 GPa)	K1 1c (0.500, 0.500 ,0.500) K2 2g (0.500, 0.000, -z) z=-0.245 Cl1 1b (0.500, 0.500, 0.000) Cl2 4j (x, 0.000, z) x=0.252, z=0.747
Metallic $K_{n+1}Cl_n$, B2-layered	K_2Cl	56-300	$I4/mmm$	a = 2.749 Å c = 7.587 Å (200 GPa)	K1 4e (0.000, 0.000, z) z=0.330 Cl 2a (0.000, 0.000, 0.000)

superstructures	K_3Cl_2	80-300	*I*4/*mmm*	*a* = 2.801 Å *c* = 12.806 Å (200 GPa)	K1 2b (0.500, 0.500, 0.000) K2 4e (0.500, 0.500, z) z = 0.798 Cl 4e (0.000, 0.000, z) z = 0.897
	K_4Cl_3	62-264	*I*4/*mmm*	*a* = 2.791Å *c* =18.190Å (200 GPa)	K1 4e (0.000, 0.000, z) z=0.072 K2 4e (0.000, 0.000, z) z=0.784 Cl1 2b (0.000, 0.000, 0.500) Cl2 4e (0.000, 0.000, z) z= 0.646
	K_5Cl_4	100-255	*I*4/*mmm*	*a* = 2.789Å *c* = 23.531Å (200 GPa)	K1 2a (0.500, 0.500, 0.500) K2 4e (0.500, 0.500, z) z = 0.612 K3 4e (0.500, 0.500, z) z=0.276 Cl1 4e (0.000, 0.000, z) z=0.669 Cl2 4e (0.000, 0.000, z) z=0.557
Metallic layered fcc-superstructure	K_3Cl	149-300	*I*4/*mmm*	*a* = 3.427Å *c* = 6.714 Å (200 GPa)	K1 2b (0.500,0.500,0.000) K2 4d (0.500,0.000,0.250) Cl 2a (0.000,0.000,0.000)